International Journal of Steel Structures
March 2012, Vol 12, No 1, 93-106
DOI 10.1007/s13296-012-1009-Y

International Journal of
STEEL
STRUCTURES
www.springer.com/journal/13296

Experimental and Analytical Studies on Buckling-Restrained Knee Bracing Systems with Channel Sections

Jiuk Shin[1], Kihak Lee[2]*, Seong-Hoon Jeong[3], Han-Seon Lee[4], and Jinkoo Kim[5]

[1]*Building Research Department, Korea Institute of Construction Technology, Korea*
[2]*Department of Architectural Engineering, Sejong University, Korea*
[3]*Department of Architectural Engineering, Inha University, Korea*
[4]*Shool of Civil, Environmental and Architectural Engineering, Korea University, Korea*
[5]*Department of Architectural Engineering, Sungkyunkwan University, Korea*

Abstract

In this paper, Buckling-Restrained Knee Bracing (BRKB) system was developed through sub-assemblage tests. The core plate of the BRKB was restrained with two channel sections. Tests of the five BRKBs were carried out under cyclic loading as specified in the AISC (2005) Seismic Provisions. It was observed that the ductility and energy dissipation capacity of the BRKBs were mainly affected by the variables: size of core plate, size of channel sections, and size of end plate. Four out of five specimens satisfied the compression-strength adjustment factor and cumulative plastic ductility specified in the provisions. The BRKB, which showed the best performance among the test specimens, was applied to a piloti type reinforced concrete building. Static pushover and non-linear time history analyses were performed to confirm the retrofit effect. The analysis results showed that the installation of the BRKBs improved the seismic behavior of the building significantly in terms of strength and story drift.

Keywords: buckling-restrained knee brace, sub-assemblage test, piloti type reinforced concrete building, seismic retrofit

1. Introduction

The construction of multi-unit residential building structures has recently increased rapidly with urban population growth in Korea. Residential buildings in Korea can be classified into high-rise buildings with large unit area and low-rise buildings with small unit area. In the most low-rise buildings existing in Korea, seismic design requirements have not been enforced. Currently retrofitting those existing low-rise RC buildings against earthquake loading is an important issue in Korea. Fig. 1 shows a typical non-seismic low-rise residential building located in Korea. This five story RC residential building is composed of moment frames in the 1st story and shear wall system in the upper stories. The open space piloti in the first story is often used as a parking area, and thus the addition of diagonal/X-bracing or shear walls may not be an option for seismic retrofit.

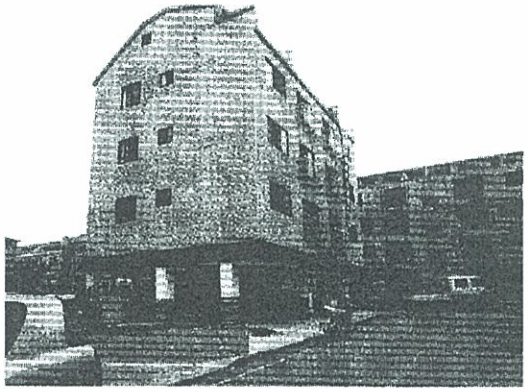

Figure 1. Typical view of a low-rise residential building in Seoul, Korea.

The present study investigates the use of a steel knee bracing for seismic retrofit of a low-rise multi-unit residential structure. Since steel knee bracing can be installed in proximity to the beam-column joint area, they do not restrict the parking area. In addition, ease of constructability of the knee bracing system, in contrast to the addition of shear walls, makes it possible to carry out the seismic retrofit without any inconvenience to residents

Note.-Discussion open until August 1, 2012. This manuscript for this paper was submitted for review and possible publication on December 15, 2011; approved on March 2, 2012.

*Corresponding author
Tel: +82-3408-4331; Fax: +82-3408-3331
E-mail: kihaklee@sejong.ac.kr

as demonstrated in the previous studies (Balendra *et al.*, 1991; Suita *et al.*, 2006). However, bracing systems are generally vulnerable to cyclic loadings such as earthquake ground motions, due to buckling under compression. Thus a buckling-restrained brace (BRB) is considered in this study, which shows large inelasticity without buckling under compression. The detailed information of BRBs is given in elsewhere (Takeuchi *et al.*, 2010).

Many researchers have carried out experiments and numerical analyses of BRBs for incorporation into a seismic force resisting system. Yoshino and Karino (1971) performed tests on a brace element comprised of a flat steel plate (a core plate) and reinforcing concrete panels (as a restrainer) with debonding material. The debonding material was used to avoid attachment between the core plate and the restrainer. Watanabe *et al.* (1988) found that the elastic buckling strength of the restrainer should be larger than the yield force of the core plate for preventing overall flexural buckling of the BRB. Studies on practical applications of BRB to buildings were conducted by Qiang (2005), and design procedures incorporating BRBs into building structures were suggested by Clark *et al.* (1999) and Choi and Kim (2009). Modeling of hysteretic curves by component tests of BRBs was carried out by Black *et al.* (2004). From the tests and analysis results, it was concluded that a BRB can be used as a practical and reliable alternative to conventional lateral load resisting systems. A new type of BRB, a double-Tee double-tube BRB (DT-BRB), was suggested by Tsai *et al* (2002). Pseudo-dynamic experiments and numerical analyses of a large scale frame with BRBs were conducted by Fahnestock *et al.* (2004), and it was found that the connection at the ends of the BRB should have sufficient stiffness and strength for maintaining stable behavior under maximum compression and tension force.

Experimental and analytical studies of a knee brace system were performed by many researchers. Aristizabal-Ochoa (1986) developed a Knee Braced Frame (KBF) as a new alternative structural system for earthquake-resistant steel buildings. Sam *et al.* (1995) carried out pseudo-dynamic testing of single and double story KBF models, and showed that the knee brace systems were enough to reduce the damage due to the earthquake loadings effectively and economically. Pushover test of a knee brace and X-brace systems installed into a RC moment frame was performed by Maheri *et al.* (2003). They also evaluated the response modification factors of the steel X-braced and knee-braced RC buildings, and showed that the steel-braced RC frame possessed much larger ductility capacity than that of an unbraced RC building. Kim and Seo (2003) evaluated the seismic performance of a moment frame installed with buckling-restrained knee braces, and found that the BRKB could be an effective system for seismic retrofit of moment resisting frames.

The aim of the present research is to develop a buckling restrained knee bracing (referred to as BRKB) systems composed of a steel core plate restrained by channel sections. For a typical BRB or BRKB, buckling is inhibited by a concrete or mortal filled steel tube. However, the BRKB system developed in this study uses the steel channel sections as a restrainer. The developed system was to increase the quality in manufacturing process, and have flexibility in the design details at both ends of the core plate. The BRKBs are installed in a 1-bay 1-story steel frame and tested under cyclic loading to verify the seismic performance. Then an analytical model for a non-seismic designed low-rise RC building retrofitted with BRKBs is evaluated using pushover and nonlinear time history analyses to validate the effectiveness of the proposed BRKBs for seismic retrofit.

2. Design of a Buckling-Restrained Knee Brace

In this study, a total of five BRKB specimens were manufactured and tested under cyclic load. Design variables for the five test specimens were the size of the core plate (aspect ratio of the core plate), the size of the channel sections (or P_{cr}/P_y), and the size of the end plate (aspect ratio of the end plate). Details of the specimens are summarized in Table 1, where the letters C and R in the naming of the specimens denote the core plate and the channel sections, respectively. The numbers following C and R represent the width of the core plate and the web length of the channel section, respectively. Dimensions and drawing details of a typical specimen used for this study are shown in Fig. 2. In Fig. 2, the core plate was designed to resist the axial force transmitted to the brace, and the channel sections were used to restrain the core plate from buckling. Debonding material (rubber) was

Table 1. Properties of the BRKB test specimens (unit: mm)

Specimen	Core plate		Channel section			End plate		Stiffener	
	Dimension	Aspect ratio	Dimension	P_{cr}/P_y	Groove length	Dimension	Aspect ratio	Dimension	Clearance
C42R100-1	42×16	2.60:1	100×50×5×7.5	2.53	310	160×19	8.40:1	80×60	280
C42R100-2	42×16	2.60:1	100×50×5×7.5	2.53	310	120×19	6.30:1	80×60	280
C42R150-R	42×16	2.60:1	150×75×6.5×10	9.41	350	160×19	8.40:1	80×60	300
C60R100	60×16	3.75:1	100×50×5×7.5	1.78	310	160×19	8.40:1	80×60	280
C60R150	60×16	3.75:1	150×75×6.5×10	6.59	310	160×19	8.40:1	80×60	280

used for minimizing friction occurring between the channel sections and core plate. Guide plates were added to each specimen to prevent buckling of the end plates. Grooves at the ends of the channel section were cut in order to prevent contact between the guide plates and the channel sections.

For the design of the BRKB, the maximum of axial force of the core plate was assumed as the maximum capacity of an actuator used in this test, and 42×16 mm (2.60:1) and 60×16 mm (3.75:1) core plates were designed using ductility demands of the brace calculated by 1.50% and 3.0% allowable inter-story drift ratio, respectively. The sizes of the channel sections were determined based on the findings from the previous research performed by Watanabe *et al.* (1988) who suggested that the yield strength (P_y) of the core plate should be larger than the buckling strength (P_{cr}) of the channel section ($P_{cr}/P_y>1.0$) to prevent buckling of the core. For the specimen with the 42×16 mm core plate, two different P_{cr}/P_y of the channel sections were used; i.e. P_{cr}/P_y=2.53 (100×50×5×7.5 mm) and P_{cr}/P_y=9.41 (150×75×6.5×10 mm). For the specimen with the 60×16 mm core plate, P_{cr}/P_y of the channel sections corresponded to 1.78 (100×50×5×7.5 mm) and 6.59 (150×75×6.5×10 mm). In this study, the dimension of the non-retrofitted parts including the end plate was determined using Eq. (1) proposed by Tsai and Weng (2002) for preventing buckling of the parts. They showed that the buckling strength of the ends of the brace, computed using the following equation, should be larger than the maximum compression force:

$$P_{e\_trans}=\frac{\pi^2 EI_{trans}}{(KL_n)^2}\times P_{max} \quad (1)$$

where P_{e_trans} is the buckling strength of the end of the brace, I_{trans} is the second moment of inertia of the end of the core plate, and L_n is the length of the non-retrofitted section. In order to connect the two restrainer channel sections, 80×60 mm stiffeners were welded to the channel sections at a uniform interval. The stiffeners were welded at the top and bottom of the channel sections. The number of stiffeners was determined such that the buckling of the parts between the stiffeners would be prevented under the maximum compressive forces. In order to prevent the local buckling, it is very important that only steel-encased BRBs minimize friction forces occurring between the core plate and channel sections. Tremblay *et al.* (2006) discussed the role of a gap between the core plate and the steel restrainer in both directions, and Mehmet and Cem (2010) used four layers of 0.05 mm-thick polyethylene film and grease in order to reduce the frictional force. In this study, instead of providing a gap, a 2 mm-thick rubber sheet was placed as a debonding material between the core plate and the channel sections as depicted in Fig. 2. The yield stress and the ultimate strength of the test specimens obtained by coupon test are shown in Table 2, where it can be observed that the yield and ultimate stresses of the specimens are slightly higher than the nominal values for the SS400 steel used for the specimens (σ_y=235 MPa, σ_u=400 MPa).

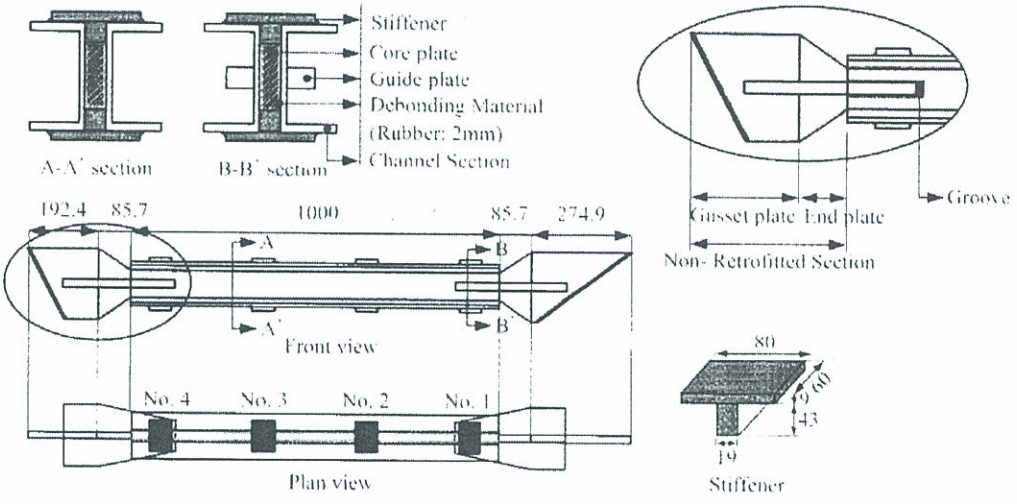

Figure 2. Details of a typical specimen.

Table 2. Result of property test

Specimen	Thickness (mm)	Width (mm)	Yielding stress (MPa)	Ultimate stress (MPa)
Gusset plate	19	40	267.4	437.6
Core plate	16	40	278.3	436.7

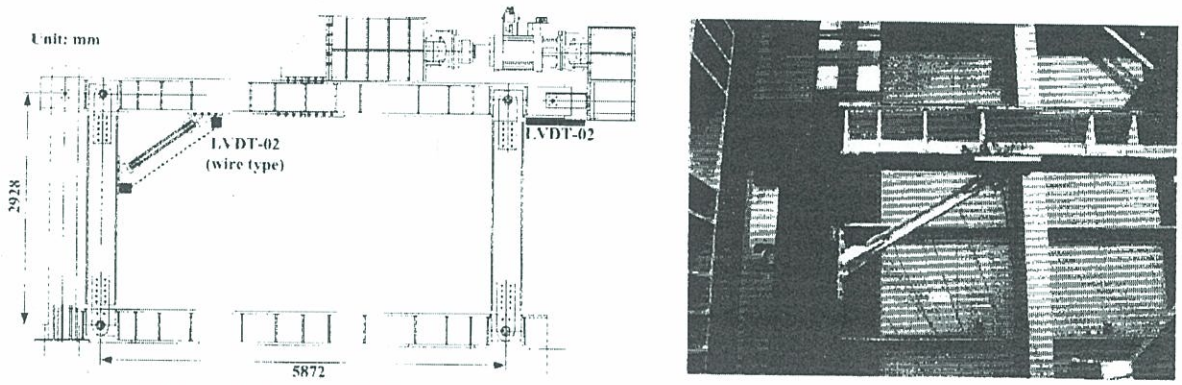

(a) Schematic drawing (LVDT location) (b) Photograph of the specimen

Figure 3. Schematic drawing & photograph of test setup.

3. Test Plan and Specimen Installation

A schematic drawing and a photograph of the pin-connected 1-bay 1-story test frame (5.87 m×2.93 m) with a BRKB specimen are shown in Fig. 3. Bearings were placed at the upper and lower joints of the vertical steel member to simulate desired behavior of the pin connection. With this configuration, only the BRKB resist lateral loading, and thus the loading is not transferred to the supporting frame. Cyclic loading was applied to the frame with a hydraulic actuator installed between the upper horizontal loading frame and the reference wall (Fig. 3). The loading step of each specimen was determined by the specifications of the AISC (2005) as illustrated in Fig. 4 and listed in Table 3. The loading protocol was established up to 3.0% of the inter-story drift ratio of the steel frame. This is twice the maximum design story drift (Δ_{bm}) specified in the AISC Seismic Provisions, which is 1.5% of the story height. The first set of the loading cycles (1st and 2nd steps in Table 3) was applied to the test frame within an elastic range. This is intended to reduce experimental error and allow observation of the initial behavior of the brace prior to plastic deformation. Two cycles of loading were applied for each target drift of 0.75, 1.5, 2.25, and 3.0% inter-story drift ratios. After

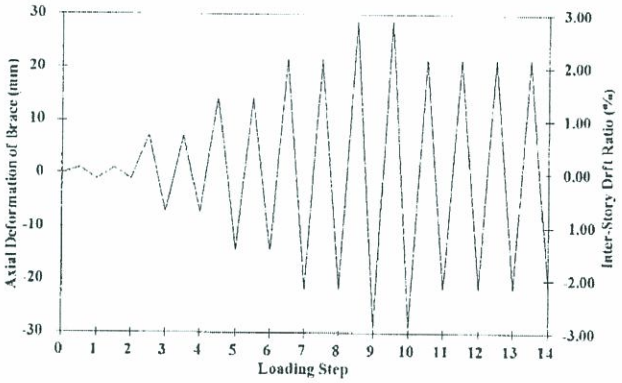

Figure 4. Loading protocol specified in the AISC Seismic Provisions.

reaching 3.0% of the inter-story drift ratio, four cycles of 2.25% inter-story drift (11th-14th loading steps in Table 3) were additionally applied to the test frame in order to satisfy the AISC (2005) specification, which requires the cumulative inelastic strain more than 200 times of the yield strain. Afterwards, if the brace had not fractured within the above AISC (2005) loading steps (1st-14th loading steps), the ultimate resisting capacity of the brace was investigated by applying four loading steps (15th-18th loading steps, additional loading steps in Table 3). In

Table 3. Cyclic loading step for the experiment

Steps	Cycles	Lateral deformation of frame (mm)	Axial deformation of brace (mm)	Inter-story drift ratio (%)	Comment
1-2	$2\cong\Delta_{by}$	3.31	2.81	0.11	AISC (2005) loading steps
3-4	$2\cong0.5\Delta_{bm}$	21.96	6.45	0.75	
5-6	$2\cong1.0\Delta_{bm}$	43.92	12.89	1.50	
7-8	$2\cong1.5\Delta_{bm}$	65.88	19.34	2.25	
9-10	$2\cong2.0\Delta_{bm}$	87.84	25.78	3.00	
11-14	$4\cong1.5\Delta_{bm}$	65.88	19.34	2.25	
15-18	$1\cong2.5\Delta_{bm}$	109.8	32.23	3.75	Additional loading steps
	$1\cong3.0\Delta_{bm}$	131.76	38.67	4.50	
	$1\cong3.5\Delta_{bm}$	153.72	45.12	5.25	
	$1\cong4.0\Delta_{bm}$	175.68	51.56	6.00	

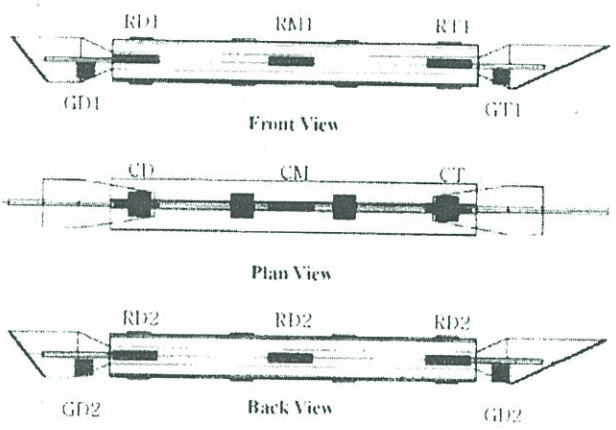

Figure 5. Location of strain gauges installed in the specimen.

each cycle of the latter loading steps, the test frame was pushed to the inter-story drift ratios of 3.75, 4.50, 5.25, and 6.0% which are 2.5, 3.0, 3.5 and 4.0 times the design story drift (Δ_{bm}), respectively. An LVDT (Linear Variable Differential Transformer) was installed at the frame to record the transverse deformation that occurred in the frame and a wire type LVDT was also placed at the end plate of the BRKB to examine the axial deformation, as shown in Fig. 3(a). This procedure was applied to reduce the slip through comparison of the lateral deformation of the frame with the deformation of the actuator. In order to measure the strains of the core plate and the channel sections, plastic strain gauges were installed at the top, center, and bottom of the brace, as shown in Fig. 5.

4. Test Results of the BRKB specimens

4.1. Hysteretic behavior and failure modes

Axial force-deformation relationships obtained from the experimental results of the five BRKB specimens are presented in Fig. 6. The failure modes of the C60R100 and C60R150 specimens are shown in Fig. 7. The C42R100-1 exhibited no significant deformation except for cracking of the plaster at the surface and rubber detachment at the upper and lower parts of the brace up to the 6th loading step (1.5% inter-story drift ratio). At the 8th loading step (2.25% inter-story drift ratio), some cracks of the plaster at the stiffeners were observed due to in-plane buckling of the core plate. The No. 2 stiffener was detached from the brace at the 10th loading step. The detachment, which was resulted in a loss of confinement, occurred due to the strong axis buckling of the core plate. The experiment was stopped due to a fracture of the core plate at the 14th loading step (four cycles of 2.25% inter-story drift ratio as shown in Table 3).

The C42R100-2 specimen served as a reference model among the five specimens. The only difference between C42R100-1 and C42R100-2 was the size of the end plate; 160×19 and 120×19 mm for C42R100-1 and C42R100-2, respectively. The C42R100-2 displayed a similar behavior to that of the C42R100-1 until the 10th loading step was reached. The core plate and the channel sections of the latter specimens did not show significant deformation up to the 6th loading step (1.5% inter-story drift ratio). At the 8th loading step (2.25% inter-story drift ratio),

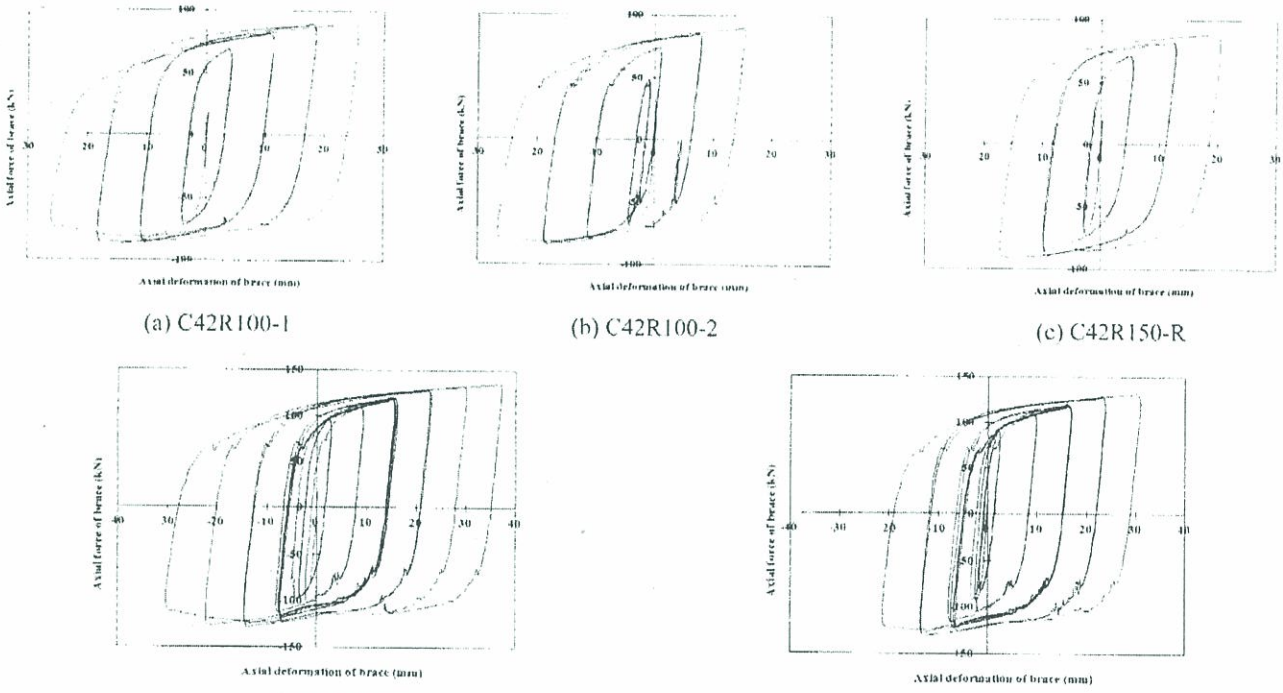

(a) C42R100-1 (b) C42R100-2 (c) C42R150-R

(d) C60R100 (e) C60R150

Figure 6. Load-displacement hysteresis curves of the BRKBs.

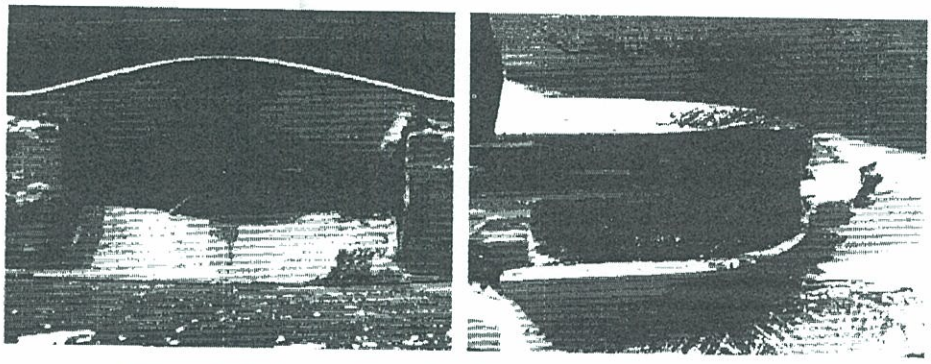

Figure 7. Failure modes of C60R100 and C60R150 specimens.

gradual in-plane buckling of the core plate was observed. After the 10th loading step (3.0% inter-story drift ratio), detachment of No. 3 stiffener was observed with an increase of the axial deformation of the specimen. Global buckling of the core plate in strong axis was observed at the 13th loading step (four cycles of 2.25% inter-story drift ratio in Table 3). The failures of the C42R100-1 and C42R100-2 occurred due to detachment of the stiffeners leading to loss of confinement of the core plate. In terms of the axial force capacities, there was less than 2% difference at each step between the C42R100-1 and C42R100-2 (Fig. 6 (a) and (b)). Through this comparison, it was observed that the size of the end plate did not significantly affect the axial force of the brace.

The C42R150-R specimen was designed with an increase of the channel section size; 150×75×6.5×10 mm compared to 100×50×5×7.5 mm of the aforementioned C42R100-1 and C42R100-2 specimens. As a result, the ratios P_{cr}/P_y for the C42R100 and C42R150-R specimens, are 2.53 and 9.41, respectively. The confinement effect of the channel sections was investigated using the two specimens. In all specimens except the C42R150-R, uniform core plate sections of 42×16 mm were used along the whole longitudinal length as a main force resisting element. On the other hand, for the C42R150-R specimen, the core plate at the ends was enlarged to 75.2×16 mm in order to enhance the buckling strength. The C42R150-R specimen showed minimal deformation up to the 6th loading step (1.5% inter-story drift ratio). Out-of-plane buckling at the ends of the core plate was observed after the 6th loading step. The brace was fractured under the tension force at the 10th loading step (3.0% inter-story drift ratio). Unexpectedly, despite the larger size of channel sections and the core plate, the end of the C42R150-R buckled at an earlier loading step. In this specimen the guide plate was designed longer than other specimens; as a result, the groove length of the C42R150-R had to be designed longer than those of other specimens. Due to the longer groove length, larger stresses were concentrated at the groove and the specimen failed in an earlier loading stage.

The width of the core plate was increased in the C60R100 specimen compared to the three C42R specimens. As shown in the hysteresis curve of Fig. 6(d), it displayed the most stable hysteretic behavior among all five test specimens as well as the best energy dissipation capacity. It also showed no significant deformation up to the 8th loading step (2.25% inter-story drift ratio). Cracks of the plaster at the surface of the channel sections occurred at the 10th loading step (3.0% inter-story drift ratio). However, only a few cracks were observed visually at the stiffeners, channel sections, etc. up to the 14th loading step (four cycles of a 2.25% inter-story drift ratio in Table 3). After applying additional loading steps, in-plane buckling of the core plate was observed at an inter-story drift ratio of 3.75%. Significant deformation was observed at No. 2 and No. 3 stiffeners at the 16th loading step (4.5% inter-story drift ratio), as shown in Fig. 7. Local buckling of the channel sections occurred with deformation of the stiffeners. Although in-plane and out-of-plane buckling of the core plate occurred at the additional loading steps, the core plate still remained and was well restrained by the channel sections and stiffeners. Finally, fracture of the core plate occurred at the 17th loading step (5.25% inter-story drift ratio), with axial displacement of 45.12 mm under the tension force.

The specimen C60R150 with a core plate of 60×16 mm (aspect ratio=8.42:1) and two channel sections of 150×75×6.5×10 mm (P_{cr}/P_y=6.59) was designed to have larger channel sections than the specimen C60R100 in order to investigate the confinement effect of the channel sections. As shown in Fig. 6(e), the hysteresis curve is stable and excellent energy dissipation capacity similar to that of the specimen C60R100 was obtained. The hysteresis loops of the C60R150 showed asymmetric shapes between the tension and compression. The asymmetric hysteresis loops were attributed to the slips occurring during the test. The specimen underwent no significant deformation until the 10th loading step (3.0% inter-story drift ratio); only cracking of the plaster on the surface of the channel sections was observed. Cracks of the plaster of the stiffeners and deformation of the core plate started at the 12th loading step (four cycles of 2.25% inter-story drift in Table 3). Before the additional loading steps (15th-18th

loading steps in Table 3) were applied, there was no significant deformation in the channel sections. As the C60R150 specimen was composed of larger channel sections than those of the specimen C60R100, it was expected that the performance of the former would be better than that of C60R100. However, this specimen failed to exhibit full capacity due to local buckling at the end of the channel sections. During the test the rubber sheet at the end of the core plate was detached followed by the damage at the end of the core plate. When the additional loading steps were applied, an end of the core plate buckled and then the specimen fractured at the 16th loading step (5.25% inter-story drift ratio) as shown Fig. 7(b).

4.2. Compression-strength adjustment factor (β)

The AISC Seismic Provisions (2005) specifies the compression-strength adjustment factor (β) for BRBs. The β factor is the ratio of the maximum compression strength to the maximum tension strength of the test specimen, measured from qualification tests for a range of deformations corresponding to 2.0 times the design story drift. The compression strength of a BRB is generally larger than the tension strength due to the confinement of the restrainers. For inverted-V-type bracing, when the β factor is too large, the beam intersected by the BRB can be fractured due to unbalanced force in the vertical direction. The Seismic Provisions specify that the β factor should not exceed 1.3.

Based on the experimental results, the β factor of the BRKB specimens was calculated and the results are presented in Fig. 8. The β factors for C42 and C60 specimens are depicted in Fig. 8(a) and 8(b), respectively. Overall, the specimens satisfied the limit of the β factor specified in the Seismic Provisions. The β factor gradually decreased when the axial deformation of the brace increased due to local buckling at the channel sections. Fig. 8(a) shows that the β factor of the specimen C42R150-R was larger than those of the specimens C42R100-1 and C42R100-2. Fig. 8(b) shows that C60R150 has a larger β factor than C60R100 during the specified loading steps. However, after the additional loading steps, the β factor of the specimen C60R150 steeply declined. This was because the specimen could not resist the compression force from the additional loading steps due to buckling at the end of the core plate.

4.3. Comparison of plastic ductility (μ) of the specimens

The cumulative plastic ductility (CPD) of each specimen was calculated by summation of the ductility of each cycle. The cumulative plastic ductility was obtained by a ratio of the difference between the maximum tension deformation ($u_{pi}^{\max}$) and the maximum compression deformation ($u_{pi}^{\min}$) over the yield deformation (u_y) with respect to each loading cycle as defined in the AISC Seismic Provisions (2005) and in the AISC-SEAOC (Structural Engineers Association of California) Recommended Provisions for Buckling-Restrained Braced Frames (2005). The Seismic Provisions stipulate that the brace test specimen must achieve a cumulative inelastic axial deformation of at least 200 times the yield deformation (more than the cumulative plastic ductility of 200). The Recommended Provisions for Buckling-Restrained Braced Frames require that the cumulative plastic ductility of the BRB be at least 140 times the yield deformation.

In this study, it was observed that four specimens (C42R100-1, C42R100-2, C60R100 & C60R150) exceeded the cumulative plastic ductility of 140 specified in the AISC-SEAOC (Fig. 9(b)) while all specimens did not satisfy the CPD requirement of AISC Seismic Provisions (Fig. 9(a)). When the additional loading steps were used, C60R100 and C60R150 specimens exceeded the CPD requirement of the AISC. Unlike a component test, the sub-assemblage test may have a difficulty involved with the connection between brace and test frame. In this study, unexpected slips occurred in the connections during the sub-assemblage test which significantly affected the test results. As shown in Fig. 6, the axial deformation of some specimens at each loading step was directed toward compression or tension side due to the slips, which resulted in the reduced CPD within the specified loading

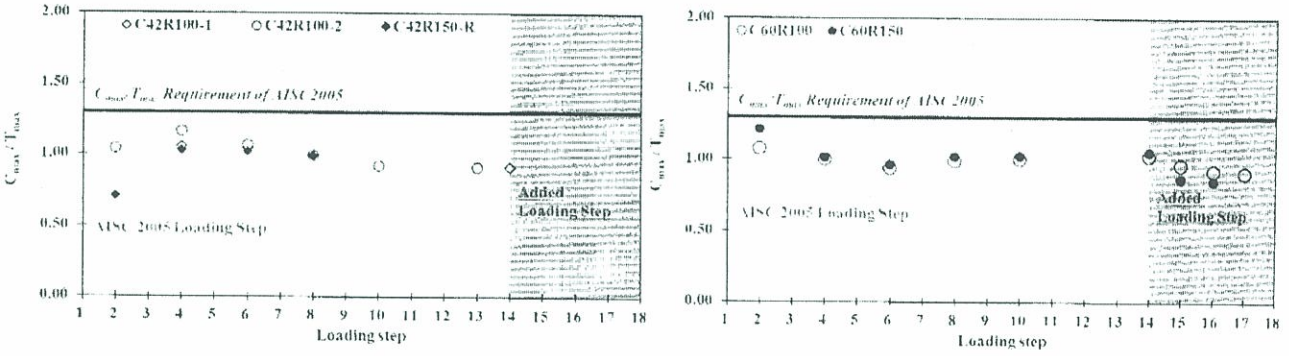

(a) C42 specimens (42x16 mm core plate) (b) C60 specimens (60x16 mm core plate)

Figure 8. Compression-strength adjustment factor for the C42 and C60 specimens.

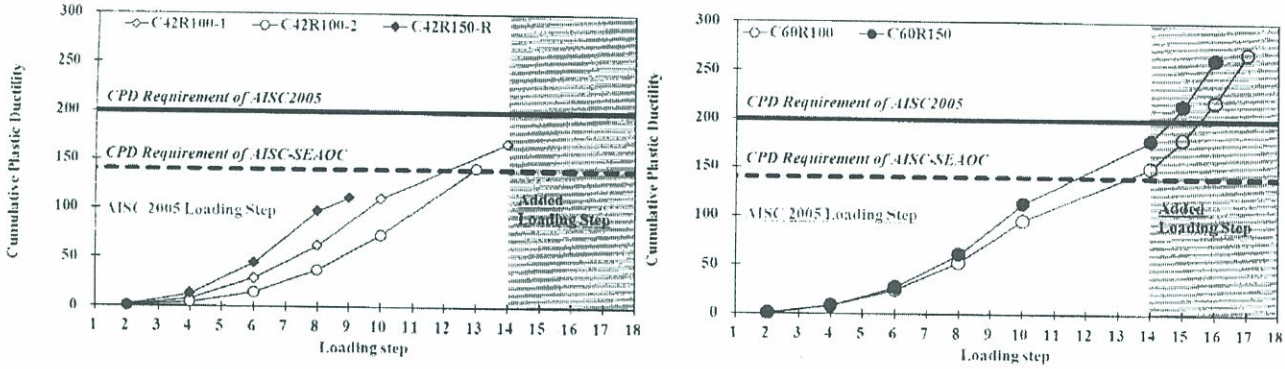

(a) C42 specimens (42x16 mm core plate) (b) C60 specimens (60x16 mm core plate)

Figure 9. Cumulative plastic ductility of the C42 and C60 specimens.

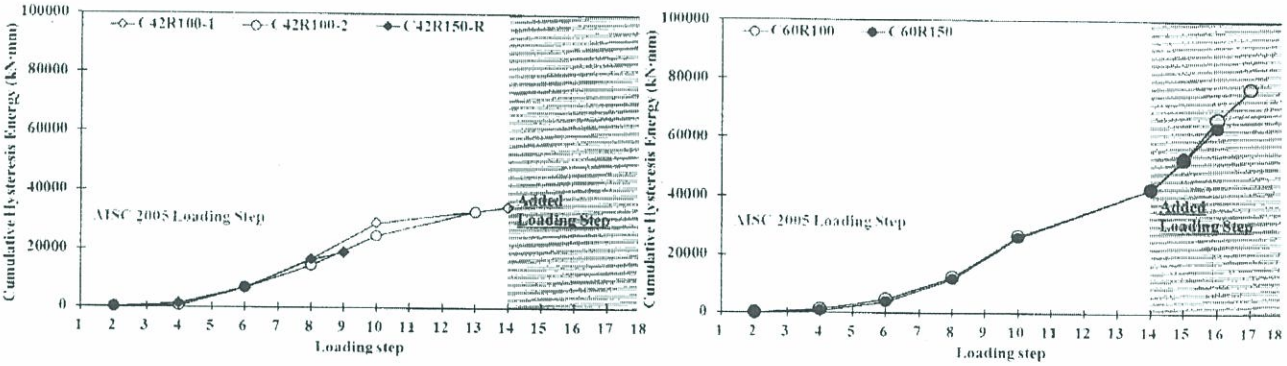

(a) C42 specimens (42x16 mm core plate) (b) C60 specimens (60x16 mm core plate)

Figure 10. Cumulative hysteretic energy of the C42 and C60 specimens.

steps. It should be noted that the cumulative plastic ductility in the Seismic Provisions is required only for the BRB component test, not for the sub-assemblage test. Therefore the test results obtained in this study do not imply that the seismic performance of the specimens is not satisfactory.

The cumulative plastic ductility computed for each specimen is shown in Fig. 9. In Fig. 9(a), C42R150-R has the largest ductility until the 8th loading step (2.25% inter-story drift ratio), but the ductility of C42R150-R declined starting from the 10th loading step (3.0% inter-story drift ratio). This is due to the fracture at the end of the core plate resulting from concentrated stresses around the groove. Both C42R100-1 and C42R100-2 specimens were satisfied based on the requirement of cumulative plastic ductility specified in the AISC-SEAOC. The cumulative plastic ductility of C60 specimens is shown in Fig. 9(b). While both specimens failed to satisfy the cumulative plastic ductility of 200 specified in the Seismic Provisions within the loading step, they met the CPD requirement of AISC-SEAOC (more than 140). The two specimens showed a similar trend for cumulative plastic ductility. The cumulative plastic ductility of the C60R150 specimen was larger than that of the C60R100 due mainly to the improvement of the confinement with increase of the size of the channel sections.

4.4. Comparison of energy dissipation capacity

Energy dissipation capacity was computed by the area surrounded by the load-displacement hysteretic curve of each specimen and then the cumulative hysteretic energy was computed by summing the energy dissipation capacity of the specimen with respect to each cycle as described in Horie and Yabe (1993) and Black *et al.* (2004). Fig. 10 shows the cumulative hysteretic energy of each test specimen. Among the C42 specimens, the C42R100-1 showed the most stable hysteretic curve and the largest energy dissipation. The specimen C42R150-R showed similar energy dissipation capacity to C42R100-2 specimen before fracture of the core plate. However, after fracture of the end of the core plate at the 8th loading step (2.25% inter-story drift ratio), the energy dissipation of the specimen C42R150-R abruptly decreased. The specimen C42R100-1 displayed similar energy dissipation to C42R100-2 as can be observed in Fig. 10(a). The specimens C60R100 and C60R150 dissipated almost the same energy within the AISC loading steps, as shown in Fig. 10(b). After the additional loading steps, the energy dissipation capacity of the specimen C60R150 was less than that of C60R100 due to the occurrence of local buckling of the core plate

as a result of the reduced confinement effect of smaller channel sections (Fig. 10(b)). The C60 specimens (C60R100 & C60R150) dissipated roughly twice greater energy than C42 specimens (C42R100-1, C42R100-2, and C42R150-R).

From the test results, it was concluded that the BRKB made of a core steel plate confined with channel sections satisfied the β factor requirement of the AISC Seismic Provisions and the CPD of the AISC-SEAOC. The confinement of the channel sections was sufficient to prevent buckling at the core plate within the loading steps specified in the Seismic Provisions. Cumulative hysteresis energy of the C60R100 (76750 kN-mm) is larger than about 20% that of the C60R150 (63400 kN-mm) at the last loading step of the each test model. The C60R100 specimen showed the best load resisting capacity among the five specimens. This specimen had the largest cumulative energy dissipation capacity and satisfied the requirements for the β factor and cumulative plastic ductility specified in the provisions during the loading steps used in the experiment (AISC loading steps & additional loading steps). In the following section, a numerical analysis of a reference building retrofitted with the C60R100-type BRKB was performed to investigate the effects of seismic retrofit.

5. Seismic performance of a Low-Rise RC Structure retrofitted with BRKBs

5.1. Analysis modeling

In order to investigate the retrofit effect of the BRKBs for low-rise residential buildings, a five story RC residential building was selected as a reference structure. Figure 11 shows an overview of the low-rise building analysis structure which is a typical low-rise residential building with a weak first story. The first story (RC moment frame) of the building is generally used as a parking space. Higher stories designed with shear walls are used as residential area. Since the lateral stiffness of the first story is lower than the remaining stories, deformation and damage tend to be concentrated at that level. Fig. 11(b) shows the location of the BRKBs installed for seismic

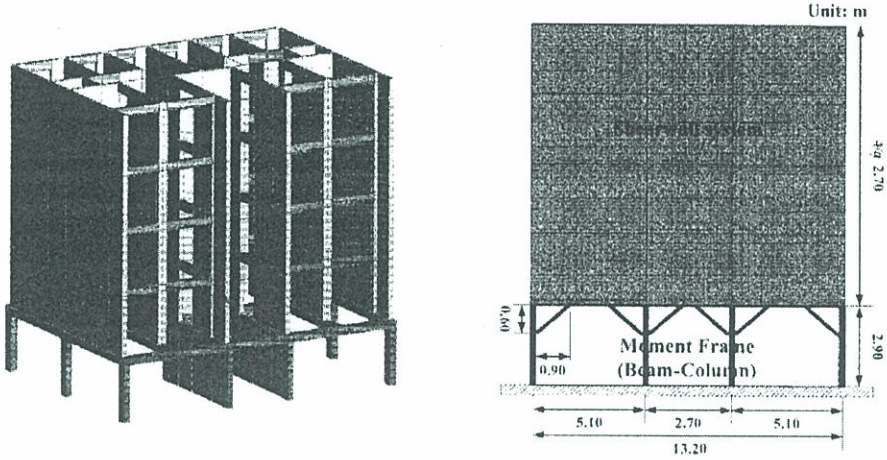

(a) 3D analytical model of the BRKB systems (b) Location of the BRKB system

Figure 11. An overview of the low-rise RC residential building.

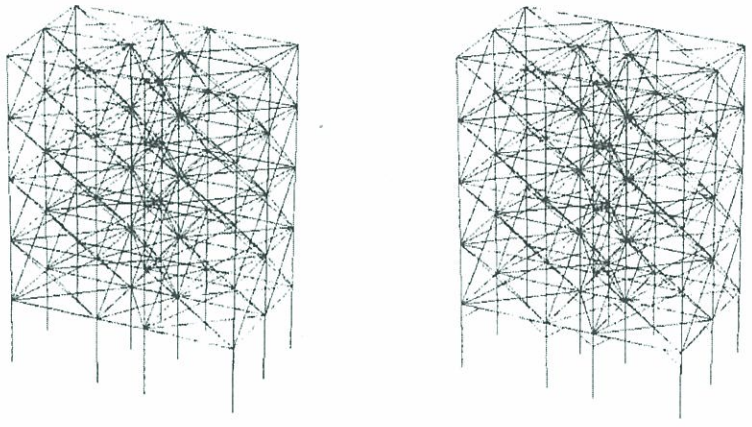

(a) As-built ZeusNL analytical model (b) Retrofitted ZeusNL analytical model

Figure 12. Analytical modes developed based on the ZeusNL program.

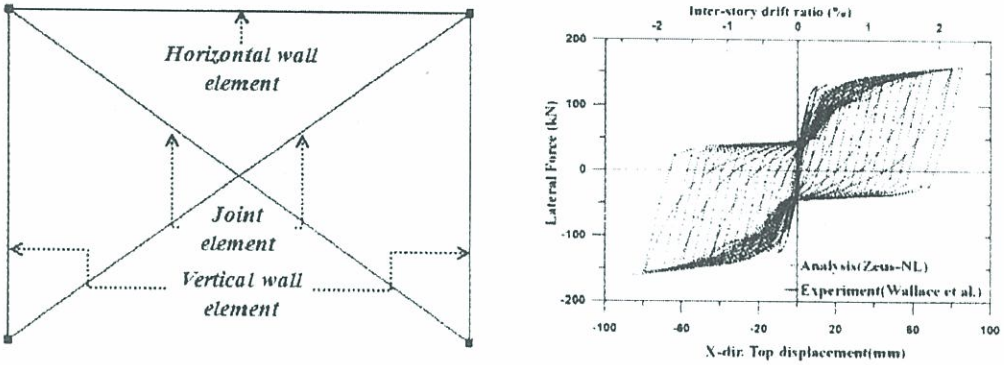

(a) Modeling of shear wall elements (b) Hysteretic behavior of a shear wall

Figure 13. Analytical modeling of a shear wall.

retrofit. Two sets of analytical models were developed; one for the as-built structure and the other for the retrofitted structure (Fig. 12) with twelve C60R100 BRKBs installed in the first story. The finite element analysis program ZeusNL (Elnashai *et al.*, 2001) was utilized to perform the analytical modeling and necessary analyses. This program is capable of representing inelasticity under static and dynamic loadings. The program has been thoroughly tested and validated over the past 20 years (Jeong and Elnashai, 2005).

Many researchers have suggested analysis models for shear wall systems, including TVLEM (Three Vertical Line Element Model) by Otani *et al.* (1985), MVLEM (Multi Vertical Line Model) by Charney (1991), column model (CM) (Kim *et al.*, 2009), and the joint element model (Stafford Smith and Girgis, 1984). This study adopted the simple method of the joint element model, which allows vertical and horizontal wall members to behave together. A flexural wall type was used for modeling shear walls. Fig. 13(a) shows the joint element model of the shear wall adopted in this study. Fig. 13(b) shows a comparison between the analytical and experimental results of the shear wall, where the solid line indicates the results from a test reported in a previous study (Orakcal *et al.*, 2006) and the dotted line is the hysteresis loop obtained from the analytical model. Since the analytical modeling is based on the center-line dimension of members, rigid arms were utilized at the beam-column joints to prevent plastic hinges within the faces of members (Fig. 14). The inelastic responses of the members are represented by fiber elements with inelastic stress-strain relationships of the materials. The connection between the steel braces and the RC moment frames was modeled by adopting rigid elements, as shown in Fig. 14 and as done in a previous study (Maheri, Kousari and Razazan, 2003). This was done to prevent sudden failure of the columns due to the retrofitting of the moment frame with the BRKBs. In order to validate the analysis model, the test result of the specimen C60R100 was compared with that of the computer model before

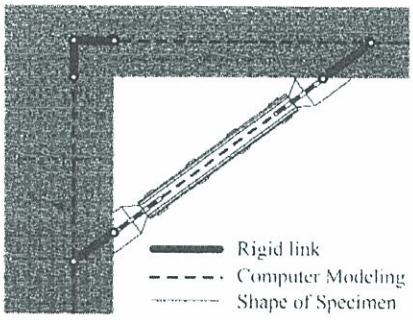

Figure 14. RC beam-column connection with the BRKB.

incorporation of the BRKBs into the analytical building model. The material properties used in the computer model, such as an initial stiffness, yield stress, and post-yield stiffness, were set to be the same with those of the test specimen. The BRKB analytical model was developed using the joint element (typical tri-linear symmetrical elasto-plastic curve type) defined in the ZeusNL as indicated in Fig. 15(a). In Fig. 15(b), the BRKB hysteresis curve developed by the ZeusNL is compared with the experimental results of the C60R100 specimen. Also, in order to compare analytical results between the BRKB and regular knee brace, the hysteresis curve of the regular knee brace was added in Fig 15(b). The size of the regular knee brace (16×60 mm, Aspect ratio=3.75:1) was the same with the BRKB (C60R100). The analytical results were measured at the same location with the experimental study. It can be observed that the analytical and experimental results are generally in good agreement in terms of maximum compression and tension force at each loading step except that the initial stiffness of the analysis model is somewhat underestimated.

5.2. Non-linear static pushover analysis

Static pushover analyses were performed to evaluate the effect of the BRKBs on the lateral load-resisting capacity of the reference building. The vertical distribution of the lateral forces on the structure was determined from

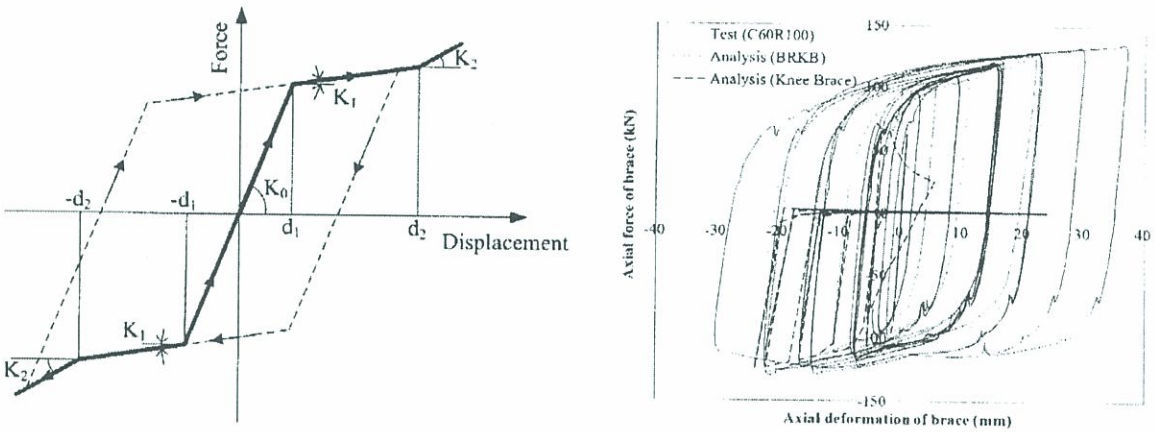

(a) Joint Element for BRKB (b) Comparison of hysteresis curves

Figure 15. Analysis modeling of the BRKB.

the seismic load distribution pattern of the International Building Code (IBC) (2009):

$$F_x = \frac{w_x h_x^k}{\sum_{i=1}^{n} w_i h_i^k} \times V \quad (2)$$

where F_x is the equivalent lateral seismic force induced at level x, V is the total design lateral force, and w_x or w_i is the portion of the total effective seismic weight of the structure assigned to level x or i. k is an exponent related to the structure period.

Figure 16 shows the load-displacement curve obtained from the pushover analysis of the analytical model before and after retrofit with the BRKBs. To meet the target performance, the size of the brace was determined in such a way that the base shear of the retrofitted building is larger than 30% of the as-built building. For increasing 30% of base shear, the size of core plate is 180×48 mm (Aspect ratio=3.75:1) and the size of channel section is 200×70×7×10 mm (P_{cr}/P_y=9.17). The pushover curves show that both the stiffness and strength increased after the retrofit.

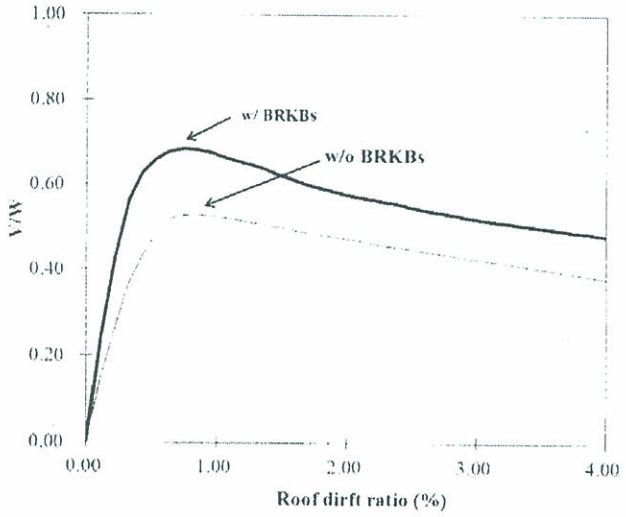

Figure 16. Result of static pushover analyses before and after retrofit.

5.3. Non-linear time history analysis

Non-linear time history analyses were carried out to investigate the responses of the reference building before and after the retrofit. The fundamental periods of as-built and retrofitted buildings are 0.69 and 0.48 sec., respectively. Ten input ground motions were selected among the twenty earthquake records used in Somerville *et al.* (1997) and were modified to the design spectrum (Stiff soil) of the KBC (Korean Building Code) 2009 (2009). The list of the selected input ground motions is given in Table 4 and the individual and mean response spectrum are presented in Fig. 17. The original earthquake records were modified using the software SeismoMatch (SeismoSoft, 2010). This program is capable of adjusting earthquake accelerograms to match a specific target response spectrum, using the wavelets algorithm proposed by Abrahamson (1992) and Hancock *et al.* (2006).

Figure 18 shows the inter-story drift ratios of the analytical models before and after the retrofit. Figure 18 (a) and (b) present the analytical results for the as-built building and the building retrofitted with the BRBKs, respectively. The dynamic analysis results included the 84 and 95% probability values as well as the median values of the responses under the ten ground motions. From the analysis results, it was observed that the inelastic behavior was concentrated in the 1st story moment frames. The maximum inter-story drift ratios for the original building were 3.47, 3.62, and 3.91% for the median, 84 and 95% probability, respectively (Fig. 18(a)). On the other hand, the maximum inter-story drift ratios for the retrofitted system were 2.51, 2.65, and 2.74% for the median, 84 and 95% probability, respectively (Fig. 18(b)). The maximum inter-story drift ratio of the analytical models occurred at the first story of the building. The reduction in the median

Table 4. List of earthquake records used in the dynamic analysis

Name	Earthquake	Time (sec.)	Step	PGA (Original)	PGA (Matched)
R1	Loma Prieta 1989	23.65	4730	0.36 g	0.42 g
R2	Kocaeli 1999	22.53	4506	0.35 g	0.42 g
R3	Kobe 1995	24.80	4960	0.35 g	0.35 g
R4	Imperial Valley 1979	39.99	3999	0.31 g	0.35 g
R5	Helena 1935	40.00	4000	0.17 g	0.44 g
R6	Friuli 1976	36.33	3633	0.35 g	0.46 g
R7	Emeryville 1989	20.52	4104	0.25 g	0.33 g
R8	Chi-Chi 1999	37.02	3702	0.36 g	0.34 g
R9	San Francisco 1957	39.72	3972	0.11 g	0.36 g
R10	Duzce 1999	41.51	4151	0.51 g	0.49 g

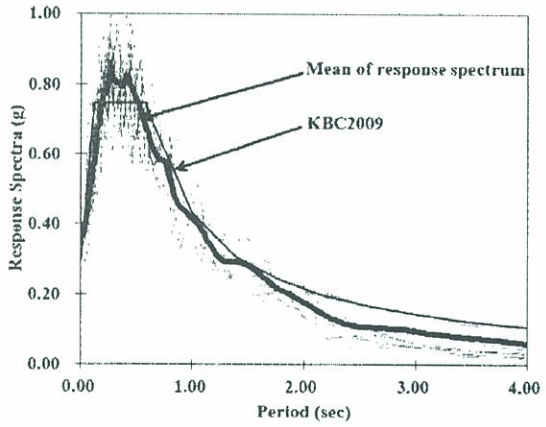

Figure 17. Response spectra of the 10 ground motions and the KBC design spectrum.

value of the maximum inter-story drift is 0.96% of the story height, which changed the damage state of the reference building from the 'Collapse' state to the 'Collapse Prevention' state according to the damage scale in the FEMA 450 (2003) where 3% inter-story drift ratio is assumed as the threshold for the collapse of RC moment frames.

Figure 19 compares of maximum inter-story drift ratios of the as-built and retrofitted buildings subjected to each of the input ground records. For most of the input ground records, the inter-story drift ratios were reduced from above 3% of the story height to below that value, which implies that collapse of the reference building can be prevented by installing the BRKBs at the first story. The retrofit effect on the shear wall system in the upper stories is marginal compared to that on the first story moment frame as shown in Fig. 19(b). Based on the above observation, it can be concluded that since the seismic inelastic behavior in the typical low-rise residential structures is concentrated on the first story moment frame, retrofit of the first story using the BRKBs can be an effective option for enhancing structural safety against earthquake loads.

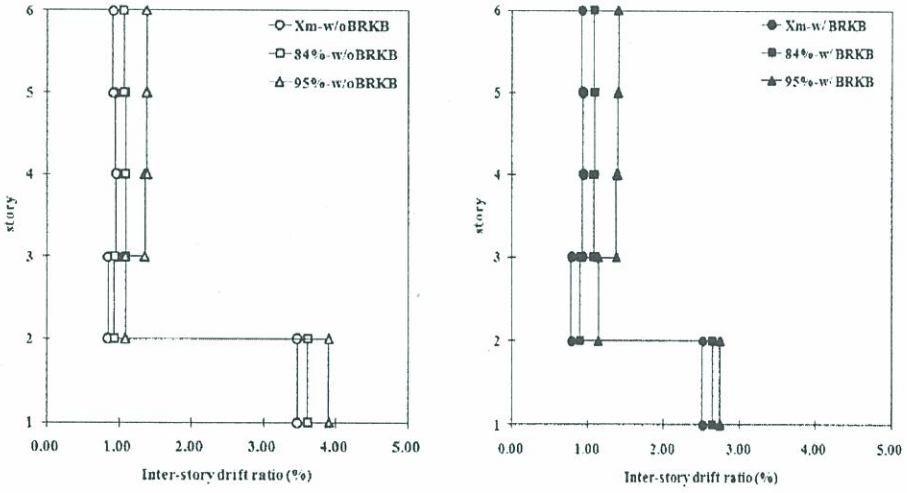

(a) As-built structure (w/o BRKB) (b) Retrofitted structure

Figure 18. Inter-story drifts of the model structure obtained from dynamic analysis.

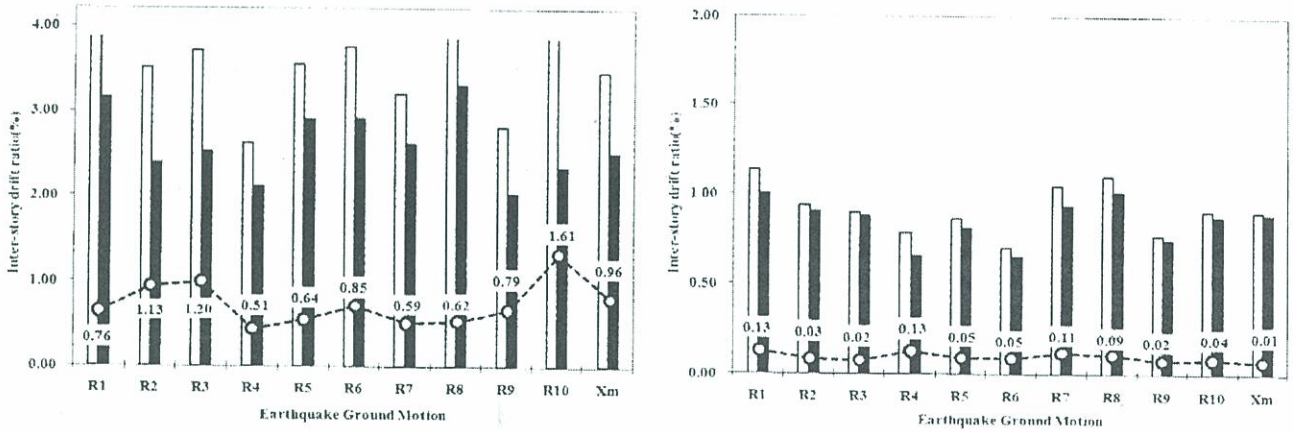

(a) Moment Frame (1st story) (b) Shear wall system (higher stories)

Figure 19. Maximum inter-story drift ratio before and after the retrofit.

6. Conclusions

Experimental and analytical studies were carried out to investigate the effect of a buckling-restrained knee brace (BRKB) for seismic retrofit of a low-rise building with weak first story. The findings of this study are summarized as follows.

In the sub-assemblage tests of the developed BRKB specimens, ductile force-displacement relationships were observed. All BRKB specimens satisfied the requirement for the compression-strength adjustment factor specified in the AISC Seismic Provisions. The cumulative plastic ductility (CPD) of the test specimens except the C42R150-R specimen exceeded the requirement (>140) specified in the AISC-SEAOC provisions; while no specimen satisfied the requirement (>200) specified in the AISC Seismic Provisions due to the unexpected slips during the sub-assemblage test.

The test results showed that the size of the core plate (aspect ratio) was the most influential parameter on energy dissipation capacities among the design variables considered in this study. At the 14th loading step, the cumulative hysteretic energy of the specimens with a 60×16 mm core plate (C60R100 and C60R150) turned out to be about two times larger than those of the specimens having a 42×16 mm core plate (C42R100-1 and C42R100-2). In addition, the size of the channel sections (or P_{cr}/P_y) affected the capacity of the BRKB. The CPD of the specimen C60R150 was about 19% larger than that of the C60R100 at the 14th loading step. It was also observed that the size of the channel sections improved the ductility capacity by increasing the confinement effect.

The specimens developed in this study showed several patterns of failure mode: Strong axis buckling of the core plate occurred in the specimens C42R100-1 and C42R100-2. These specimens failed due to the detachment of the stiffener caused by the buckling of the core plate in the strong axis. The specimen C60R100 showed weak axis buckling of the core plate due to the loss of confinement. The specimen C60R150 fractured at the connection of the end of the core and gusset plates where the rubber sheet used as unbonded material was detached. The specimen C42R150-R with longer groove length unexpectedly fractured at the early loading step.

The installation of the BRKBs in the weak story of the model structure resulted in the decrease of the median of maximum inter-story drift ratios below the threshold for the collapse limit state specified in the FEMA 450. Based on the analysis and test results, it was concluded that the application of BRKBs could be an effective method for improving the seismic performance of a low-rise building with weak first story.

Acknowledgments

This research was supported by Basic Science Research Program through the National Research Foundation of Korea (NRF) funded by the Ministry of Education, Science and Technology (Grant No. 2007-0054740 & 2011-0010384).

References

Abrahamson, N. (1992). "Non-stationary spectral matching." *Seismological Research Letters*, 63(1), pp. 30-38.

AISC (2005). *Seismic provision for structural steel building*. American Inst. of Steel Construction, Chicago, IL.

Aristizabal-Ochoa, J. D. (1986). "Disposable knee bracing: improvement in seismic design of steel frames." *J. Struct. Engng.* 112(7), pp. 1544-1552.

Balendra, T., Sam, M. T., and Liaw, C. Y. (1991). "Preliminary studies into the behaviour of knee braced frames subject to seismic loading." *Journal of Engineering structures*, 13(1), pp. 67-74.

Black, C. J., Makris, N., and Aiken, I. D. (2004). "Component testing, seismic evaluation and characterization of

buckling-restrained braces." *Journal of the Structural Engineering*, 130(6), pp. 880-894.

Charney, F. A. (1991). *Correlation of the analytical and experimental inelastic response of 1/5 scale seven-story reinforced concrete frame-wall structure, Earthquake-Resistant Concrete Structures inelastic Response and Design*. ACI Sp-127, American Concrete Institute, Detroit.

Choi, Y. and Kim, J. (2009). "Evaluation of seismic energy demand and its application on design of buckling-restrained braced frames." *Structural Engineering and Mechanics*, 31(1), pp. 93-112.

Clark, P., Aiken, I., Kasai, K., Ko, E., and Kimura, I. (1999). "Design procedures for buildings incorporation hysteretic damping devices." *Proc. the 69th Annual Convention*, SEAOC, Sacramento, USA, pp. 355-372.

Elnashai, A. S., Papanikolaou, V., and Lee, D. (2001). *ZeusNL – A program for inelastic dynamic analysis of structures*. MAE Center, University of Illinois at Urbana-Champaign, USA.

Fahnestock, L. A., Sause, R., and Ricles, J. M. (2004). "Seismic response and performance of buckling-restrained braced frames." *Journal of the Structural Engineering*, 133(9), pp. 1195-1204.

FEMA 450 (2003). NEHRP recommended provisions for seismic regulations for new buildings and other structures. *Report No. FEMA-450*, Washington, DC.

Hancock, J., Watson-Lamprey, J., Abrahamson, N. A., Bommer, J. J., Markatis, A., McCoy, E., and Mendis, R. (2006). "An improved method of matching response spectra of recorded earthquake ground motion using wavelets." *Journal of Earthquake Engineering*, 10, pp. 67-89.

Horie, T. and Yabe, Y. (1993) "Elasto-plastic behavior of steel brace with restraint system for post buckling." *Annual Technical Papers of Steel Structures, 1*, pp. 187-194, Japan.

IBC (2009). *International Building Code (IBC)*. International Code Council, Inc.

Jeong, S. and Elnashai, A. S. (2005). "Analytical assessment of an irregular RC frame for full-scale 3D pseudo-dynamic testing Part 1: Analytical model Verification." *Journal of Earthquake Engineering*, 9(1), pp. 95-128.

KBC 2009 (2009). *Korea building code 2009*. Architectural Institute of Korea, Korea.

Kim, J., Choi, H., and Yu, J. (2009). "Seismic capacity and construction cost of apartment buildings with various spatial flexibility." *Journal of the Architectural Institute of Korea*, 25(1), pp. 65-72.

Kim, J. and Seo, Y. (2003). "Seismic design of steel structures with buckling-restrained knee braces." *Journal of Constructional Steel Research*, 59(2), 1477-1497.

Maheri, M. R. Kousari, R., and Razazan, M. (2003). "Pushover tests on steel X-braced and knee-braced RC frames." *Journal of Engineering structures*, 25(13), pp. 1697-1705.

Mehmet, E. and Cem, T. (2010). "An experimental study on steel-encased buckling-restrained brace hysteretic dampers." *Earthquake Engng. Struct. Dyn.* 39(5), pp. 561-581.

Orakcal, K., Massone, L. M., and Wallace, W. J. (2006). Analytical modeling of reinforced concrete walls for predicting flexural and coupled-shear-flexural response. *Report No. PEER 2006/07*, Pacific Earthquake Engineering Research Center, University of California, Berkeley, CA.

Otani, S., Kabeyasawa, T., Shiohara, H., and Aoyama, H. (1985). "Analysis of the full scale seven story reinforced concrete test structure." *American Concrete Institution*, pp. 203-239.

Qiang, X. (2005). "State of the art of buckling-restrained braces in Asia." *Journal of Constructional Steel Research*, 61(6), pp. 719-724.

Sam, M., Balendra, T., and Liaw, C. (1995). "Earthquake-resistant steel frames with energy dissipating knee elements." *Journal of Engineering Structures*, 17(5), pp. 334-343.

SEAOC/AISC (2005). *Recommended provisions for buckling-restrained braced frame*, Structural Engineers Association of California/American Institute of Steel Construction.

SeismoSoft (2010). "SeismoMatch - A computer program for adjusting earthquake accelerograms to match a specific target response spectrum." http://www.seismosoft.com.

Somerville, P., Smith, N., Puntamurthula, S., and Sun, J. (1997). Development of ground motion time histories for phase 2 of the FEMA/SAC steel project. *SAC Background Document SAC/BD-97/04*, SAC Joint Venture, Sacramento, CA.

Stafford Smith, B. and Girgis, A. (1984). "Simple analogous frames for shear wall analysis." *Journal of Structural Engineering*, 110(11), pp. 2655-2666.

Suita, K., Inoue, K., Koetaka, Y., Ando, M., and Byakuno, Y. (2006). "Full-scale test on weld-free building structure with knee brace dampers." *International conference on behaviour of steel structures in seismic areas*, Stessa 2006, pp. 533-540.

Takeuchi, T., Hajjar, J. F., Matsui, R., Nishimoto, K., and Aiken, I. D. (2010). "Local buckling restraint condition for core plates in buckling restrained braces." *Journal of Constructional Steel Research*, 66(2), pp. 139-149.

Tremblay, R., Bolduc, P., Neville, R., and DeVall, R. (2006). "Seismic testing and performance of buckling restrained bracing systems." *Canadian Journal of Civil Engineering*, 33(2), pp. 183-198.

Tsai, K. C. and Weng, C. H. (2002). Experimental responses of double-tube unbonded brace elements and connections. *Report No. CEER/R91-02*, Center for Earthquake Engineering Research, National Taiwan University.

Watanabe, A., Hitomoi, Y., Saeki, E., Wada, A., and Fujimoto, M. (1988). "Properties of braced encased in buckling-restrained concrete and steel tube." *Proc. 9th World Conference on Earthquake Engineering*, Tokyo/Kyoto, Japan, pp. 719-724.

Yoshino, T. and Karino, Y. (1971). "Experimental study on shear wall with braces: Part 2. Summaries of technical papers of annual meeting." *Architectural Institute of Japan, Structural Engineering Section*, pp. 403-404.